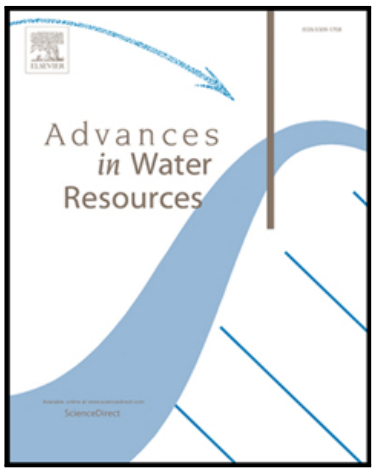

Two-Relaxation-Time Lattice Boltzmann Method and its Application to Advective-Diffusive-Reactive Transport

Zhifeng Yan, Xiaofan Yang, Siliang Li, Timothy Scheibe, Markus Hilpert

PII: S0309-1708(16)30768-0
DOI: 10.1016/j.advwatres.2017.09.003
Reference: ADWR 2936

To appear in: *Advances in Water Resources*

Received date: 11 December 2016
Revised date: 1 September 2017
Accepted date: 1 September 2017

Please cite this article as: Zhifeng Yan, Xiaofan Yang, Siliang Li, Timothy Scheibe, Markus Hilpert, Two-Relaxation-Time Lattice Boltzmann Method and its Application to Advective-Diffusive-Reactive Transport, *Advances in Water Resources* (2017), doi: 10.1016/j.advwatres.2017.09.003

Highlights

- Describes the two-relaxation-time (TRT) lattice Boltzmann method (LBM) clearly and provides a pseudocode for easy implementation
- Applies the TRT LBM to various reactive transport
- Compares the numerical stability and accuracy between the TRT LBM and the single-relaxation-time (SRT) LBM

Two-Relaxation-Time Lattice Boltzmann Method and its Application to Advective-Diffusive-Reactive Transport

Zhifeng Yan[1]

Institute of Surface-Earth System Science, Tianjin University, Tianjin, 300072, China

Xiaofan Yang

Pacific Northwest National Laboratory, Richland, WA 99354, USA

Siliang Li

Institute of Surface-Earth System Science, Tianjin University, Tianjin, 300072, China

Timothy Scheibe

Pacific Northwest National Laboratory, Richland, WA 99354, USA

Markus Hilpert

Department of Environmental Health Sciences, Columbia University, New York, NY 10032, USA

Abstract

The lattice Boltzmann method (LBM) based on single-relaxation-time (SRT) or multiple-relaxation-time (MRT) collision operators is widely used in simulating flow and transport phenomena. The LBM based on two-relaxation-time (TRT) collision operators possesses strengths from the SRT and MRT LBMs, such as its simple implementation and good numerical stability, although tedious mathematical derivations and presentations of the

[1]Corresponding author. Tel.: +86 022-27405054. yanzf14@outlook.com

TRT LBM hinder its application to a broad range of flow and transport phenomena. This paper describes the TRT LBM clearly and provides a pseudocode for easy implementation. Various transport phenomena were simulated using the TRT LBM to illustrate its applications in subsurface environments. These phenomena include advection-diffusion in uniform flow, Taylor dispersion in a pipe, solute transport in a packed column, reactive transport in uniform flow, and bacterial chemotaxis in porous media. The TRT LBM demonstrated good numerical performance in terms of accuracy and stability in predicting these transport phenomena. Therefore, the TRT LBM is a powerful tool to simulate various geophysical and biogeochemical processes in subsurface environments.

Keywords: `Lattice Boltzmann Method, Two-Relaxation-Time, pore-scale model, advection-diffusion, reactive transport, porous media`

1. Introduction

Important biogeochemical processes such as microbial metabolism and contaminant remediation take place at the pore scale in subsurface environments [1, 2, 3, 4]. Pore-scale modeling allows to directly examine the biogeochemical processes and is able to provide mechanistic insights into macroscopic field observations [5, 6]. The Lattice Boltzmann method (LBM) is one of the most widely used pore-scale methods [7, 8, 9, 10], and has been used to study various geophysical and biogeochemical processes in porous and fractured media, including solute transport [11], contaminant remediation [12, 13], geologic carbon storage [14, 15], and mineral cementation and

dissolution [16, 17, 18]. Recently, the LBM has been used to tackle more challenging problems such as heat transfer in thermofluids [19] and complex flow and reactions in nanoporous catalysts [20, 21, 22, 23].

The LBM captures the physics of macroscopic behaviors through controlling the local mesoscopic operations of pseudo-particles that move on a regular lattice, with a set of discrete velocities, and relax to an equilibrium state via a collision operator [24, 25, 7, 9, 26]. The distribution and evolution of the particles determine how the solute concentration changes with respect to space and time. The typically explicit, numerical time-stepping scheme makes it easy to develop a LBM code [27], and the local nature of the LBM makes it suitable for parallel computing [28]. Moreover, the LBM is well suited to deal with potentially reactive surface boundaries in complex pore geometries through using simple or modified bounce-back schemes [29, 30, 31, 32]. These characteristics enable the LBM to explore a variety of flow and transport phenomena in complicated geometries [9, 6].

Different selections of the collision operator result in three typical LBMs: single-relaxation-time (SRT) LBM, two-relaxation-time (TRT) LBM, and multiple-relaxation-time (MRT) LBM. These LBMs are different in terms of numerical accuracy and stability [33]. The SRT LBM employs a single relaxation parameter and is easy to implement [7]. It is the most popular LBM but may suffer from unphysical artifacts in complicated geometries and numerical instability at small relaxation rates [29, 33]. The MRT LBM employs multiple relaxation parameters, and can attain more stable and accurate simulations by tuning the relaxation parameters [34]. However, selecting the multiple relaxation parameters is challenging since it requires comprehensive

asymptotic analysis [35, 34]. The TRT LBM employs two relaxation parameters to relax the particle distributions, having one fixed but the other tunable [36, 37]. It maintains the simplicity of the SRT method in terms of implementation while retaining the advantages of the MRT method in terms of numerical accuracy and stability [33].

Since its systematic development the TRT LBM has been applied to both flow and transport phenomena [36], such as permeability estimation in different geometries [38], multi-phase flow in porous media [39, 40], advection-diffusion in bulk flow [41], and effective diffusion in unsaturated porous media [42]. However, the TRT LBM is rarely used in reactive transport, which is of great significance for many biogeochemical processes in subsurface environments [43]. The TRT method is also much less used than the SRT and MRT LBMs, although it integrates the simplicity of the SRT method and the stability of the MRT method. One reason is that the tedious mathematical derivations and presentations of the TRT method hinder its understanding and implementation [36, 44, 45, 46]. Therefore, a clear presentation of the TRT LBM is necessary for extending its applications to a broader variety of flow and transport phenomena.

This paper aims to articulate the framework and implementation of the TRT LBM as simply as possible and to apply this method to various transport phenomena. We provide a clear description of the TRT LBM including a pseudocode for straightforward implementation. The method was applied to a variety of transport phenomena to demonstrate its ability to reproduce subsurface phenomena. Advective-diffusive-reactive transport in uniform flow, for which analytical solutions are available, was examined to evaluate the

stability and accuracy of the TRT method used in simple geometries. Taylor dispersion in a pipe was examined to assess the effect of solid boundaries on the stability and accuracy. Solute transport in a packed column was examined to assess the numerical performance of the TRT method in complicated geometries. Lastly, bacterial chemotaxis in porous media was examined to illustrate the application of the TRT method to biogeochemical reactions in subsurface environments.

2. Methods

The thermodynamic state of a solute in the TRT LBM is defined by a Q-dimensional particle distribution function, $f_q(\mathbf{r}, t)$, where $q = 0, \ \ldots, \ Q-1$. This function is defined at each lattice node ($\mathbf{r}$) and for each discrete time (t). The nodes in the lattice space are connected by a set of discrete velocities $\mathbf{c}_q$ which are aligned with lattice axes and diagonals. Summing up the particle distributions over all the discrete velocities yields the solute concentration C:

$$C = \sum_{q=0}^{Q-1} f_q \tag{1}$$

At each node, the particle distribution function can be decomposed into symmetric and antisymmetric components,

$$f_q = f_q^+ + f_q^- \tag{2}$$

where $f_q^+ = (f_q + f_{\overline{q}})/2$ and $f_q^- = (f_q - f_{\overline{q}})/2$. The integer $\overline{q}$ is the index of velocity $\mathbf{c}_{\overline{q}}$ that points to the opposite direction of $\mathbf{c}_q$ ($\mathbf{c}_{\overline{q}} = -\mathbf{c}_q$). For the rest of the particles that have a zero velocity ($\mathbf{c}_0 = 0$), $f_0^+ = f_0 = C - \sum_{q=1}^{Q-1} f_q$ and

$f_0^- = 0$. In order to simplify the sums over all velocities $\mathbf{c}_q$, we assume that the velocities are ordered such that $\overline{q} = q + (Q-1)/2$ for $1 \le q \le (Q-1)/2$. Therefore $f_0^+ = C - 2\sum_{q=1}^{(Q-1)/2} f_q^+$.

The particles at one node move to neighboring nodes in terms of the non-zero discrete velocities $\mathbf{c}_q$ ($\mathbf{c}_q \neq 0$, $q = 1, \ldots, Q-1$), or stay at the node for $\mathbf{c}_0$. Once the particles reach the neighboring nodes, the resultant distributions are relaxed to an equilibrium state through a TRT collision operator [36]:

$$f_q(\mathbf{r} + \mathbf{c}_q, t+1) = \underbrace{f_q(\mathbf{r},t) - \frac{1}{\tau^+}(f_q^+ - e_q^+) - \frac{1}{\tau^-}(f_q^- - e_q^-)}_{\tilde{f}_q(\mathbf{r},t)} \tag{3}$$

where e_q^+ and e_q^- are the symmetric and antisymmetric components of the equilibrium particle distribution e_q ($e_q = e_q^+ + e_q^-$); τ^+ and τ^- are the symmetric and antisymmetric relaxation parameters, respectively. The entire right hand side of eq. (3) is called post-collision particle distribution $\tilde{f}_q(\mathbf{r},t)$.

The equilibrium particle distributions for a non-zero discrete velocity can be expressed by [47]

$$e_q^+ = C(t_q^{(m)} c_s^2 + t_q^{(u)}\overline{V^2} + w_q^{(u)}\|\mathbf{c}_q\|^2 \sum_{\alpha=1}^{d}(V_\alpha^2 - \overline{V^2})c_{q\alpha}^2 + \sum_{\beta\neq\alpha} \frac{V_\alpha V_\beta c_{q\alpha} c_{q\beta}}{2\sum_{j=1}^{(Q-1)/2} c_{j\alpha}^2 c_{j\beta}^2}) \tag{4}$$

and

$$e_q^- = t_q^{(a)} C \sum_{\alpha=1}^{d} V_\alpha c_{q\alpha} \tag{5}$$

where $q = 1, \ldots, (Q-1)/2$, V_α (or V_β) are the αth (or βth) Cartesian component of the advective velocity in the lattice space, $\overline{V^2} = \sum_{\alpha=1}^{d} V_\alpha^2/d$ where d is the dimensionality (i.e., $d = 3$ for a three-dimensional LBM), $c_{q\alpha}$ is the αth Cartesian component of the discrete velocity $\mathbf{c}_q$, c_s is the speed of sound,

$t_q^{(m)}$, $t_q^{(u)}$, $w_q^{(u)}$ and $t_q^{(a)}$ are weights. All these weights are non-negative and isotropic, and satisfy the isotropy conditions:

$$\sum_q w_q^{(\cdot)} c_{q\alpha} c_{q\beta} = \delta_{\alpha\beta}, \quad \sum_q t_q^{(\cdot)} c_{q\alpha} c_{q\beta} = \delta_{\alpha\beta} \tag{6}$$

where $\alpha, \beta = 1, \ldots, d$. Different selections of the weights result in different numerical stabilities [45].

The other half of the equilibrium particle distributions (for $q = (Q-1)/2+1, \ldots, Q-1$) can be calculated through the symmetric and antisymmetric relations

$$e_{\overline{q}}^{+} = e_q^{+} \quad \text{and} \quad e_{\overline{q}}^{-} = -e_q^{-} \tag{7}$$

For the rest of the particles, $e_0^{+} = C - 2\sum_{q=1}^{(Q-1)/2} e_q^{+}$ and $e_0^{-} = 0$.

To make the TRT method as simple as possible, we apply the widely used standard bounce-back (SBB) boundary condition:

$$f_{\overline{q}}(\mathbf{r}, t+1) = \tilde{f}_q(\mathbf{r}, t), \tag{8}$$

which mimics the phenomenon that a particle is reflected back into the pore domain when colliding with a solid boundary.

If there exists mass source or sink (M), the post-collision particle distributions are modified to:

$$\begin{aligned} \tilde{f}_q(\mathbf{r}, t) &= \tilde{f}_q(\mathbf{r}, t) + t_q^{(m)} c_s^2 M, \quad q = 1, \ldots, Q-1 \\ \tilde{f}_0(\mathbf{r}, t) &= \tilde{f}_0(\mathbf{r}, t) + M(1 - 2c_s^2 \sum_{q=1}^{(Q-1)/2} t_q^{(m)}) \end{aligned} \tag{9}$$

where $\tilde{f}_q$ on the right-hand-sides is defined in eq. (3). This modification enables the TRT LBM to simulate reactive transport.

A 3D lattice structure with 15 discrete velocities (D3Q15) was used in the simulations. The discrete velocities in the D3Q15 model can be described by

$$(\mathbf{c}_0, \mathbf{c}_1, \ldots, \mathbf{c}_{14}) = \begin{pmatrix} 0 & 1 & 0 & 0 & 1 & 1 & 1 & 1 & -1 & 0 & 0 & -1 & -1 & -1 & -1 \\ 0 & 0 & 1 & 0 & 1 & 1 & -1 & -1 & 0 & -1 & 0 & -1 & -1 & 1 & 1 \\ 0 & 0 & 0 & 1 & 1 & -1 & 1 & -1 & 0 & 0 & -1 & -1 & 1 & -1 & 1 \end{pmatrix}$$

where the $\mathbf{c}_q$ with $||\mathbf{c}_q||^2 = 1$ are classified as type I velocities, and the $\mathbf{c}_q$ with $||\mathbf{c}_q||^2 = 3$ are classified as type II velocities. The corresponding lattice structure is shown in Fig. 1. In this study, we selected the commonly used "hydrodynamic" isotropic weights [45]: $t_q^{(a)} = t_q^{(m)} = 1/3$, $t_q^{(u)} = 0$, and $w_q^{(u)} = 1/2$ for the type I velocities, while $t_q^{(a)} = t_q^{(m)} = 1/24$, $t_q^{(u)} = 1/8$, and $w_q^{(u)} = 0$ for the type II velocities. $c_s^2 = 3/8$ was chosen for both type I and II velocities. Consequently, the equilibrium distributions become:

$$\begin{aligned} e_q &= \tfrac{1}{8}C + \tfrac{1}{3}C\mathbf{c}_q \cdot \mathbf{V} + \tfrac{1}{2}C(\mathbf{c}_q \cdot \mathbf{V})^2 - \tfrac{1}{6}C\mathbf{V} \cdot \mathbf{V},\ \mathbf{c}_q \in I \\ e_q &= \tfrac{1}{64}C + \tfrac{1}{24}C\mathbf{c}_q \cdot \mathbf{V} + \tfrac{1}{16}C(\mathbf{c}_q \cdot \mathbf{V})^2 - \tfrac{1}{48}C\mathbf{V} \cdot \mathbf{V},\ \mathbf{c}_q \in II \\ e_0 &= \tfrac{1}{8}C - \tfrac{1}{3}C\mathbf{V} \cdot \mathbf{V} \end{aligned} \tag{10}$$

The D3Q15 model reduces to a one-dimensional model with three discrete velocities (D1Q3) in 1D simulations and to a two-dimensional model with five discrete velocities (D2Q5) in 2D simulations [47].

With the Chapman-Enskog expansion, the solutions of eq. (3) approach solutions to the following dimensionless reactive advection diffusion equation (ADE) [36]:

$$\frac{\partial C}{\partial T} + \nabla \cdot (\mathbf{V}C) = \hat{D}\nabla^2 C + M \tag{11}$$

where $\hat{D}$ is the dimensionless diffusion coefficient, $\hat{D} = (\tau^- - 1/2)c_s^2$. This dimensionless reactive ADE can be derived from the corresponding dimensional

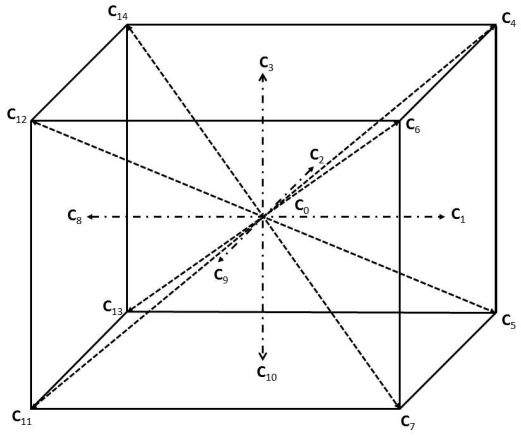

Figure 1: Lattice structure for the D3Q15 lattice Boltzmann model.

reactive ADE:

$$\frac{\partial c}{\partial t} + \nabla \cdot (\mathbf{u}c) = D\nabla^2 c + I \tag{12}$$

where c is the solute concentration ($c = c_0 C$), t is time ($t = T\Delta x/u_0$), $\mathbf{u}$ is the advective velocity of flow ($\mathbf{u} = u_0\mathbf{V}$), D is the diffusion coefficient of the solute ($D = \Delta x u_0 \hat{D}$), and I is the reaction term ($I = c_0 u_0 M/\Delta x$). c_0, Δx, and u_0 are characteristic values used to normalize the dimensional ADE.

In applications of the TRT LBM to reactive transport of a solute, the anti-symmetric relaxation parameter τ^- is determined by the diffusion coefficient of the solute, $\tau^- = 1/2 + D/(c_s^2 \Delta x u_0)$, while the symmetric relaxation parameter τ^+ is free to choose as long as $\tau^+ > 0.5$. The free selection of τ^+ enables the TRT LBM to produce robust numerical performance in terms of accuracy and stability. If τ^+ is given the same value as τ^-, the TRT method reduces to the SRT method [36, 48]. Another particular value of τ^+ is $1/2 + 1/(4\tau^- - 2)$ arose from the so-called "magic" product $(\tau^+ - 1/2)(\tau^- - 1/2) = 1/4$, which enables the TRT method to maintain good stability even for small τ^- [45].

The corresponding TRT method is called optimal TRT (OTRT) method.

The implementation of the TRT LBM to simulate advective-diffusive-reactive transport phenomena is illustrated by a pseudocode (Fig. 2). The particle distributions were updated following sequential travel and collision steps during the simulations. The dimensional concentration as a function of time is given by $c = c_0 C$.

3. Results and discussion

In this section, the TRT LBM is applied to various advective-diffusive-reactive transport phenomena, ranging from advection-diffusion in uniform flow to reactive transport in porous media. The simulation results provide insights into the applications of the TRT LBM to a variety of transport phenomena in subsurface environments.

3.1. Advection diffusion in uniform flow

One-dimensional advection-diffusion of a solute with an initially Gaussian concentration distribution was first used to evaluate the numerical stability and accuracy of the TRT method used in simple geometries. For the initial distribution

$$c(x, t = 0) = \frac{m}{\sqrt{2\pi\sigma_0^2}} \exp\left(-\frac{(x - x_0)^2}{2\sigma_0^2}\right) \tag{13}$$

the following analytical solutions can be derived [49]

$$c(x, t) = \frac{m}{\sqrt{4\pi D t + 2\pi\sigma_0^2}} \exp\left(-\frac{(x - x_0 - ut)^2}{4Dt + 2\sigma_0^2}\right) \tag{14}$$

where m is the initial mass of the solute per unit length, x_0 is the initial center of the mass, u is the advective velocity, and σ_0^2 is the variance of the initial

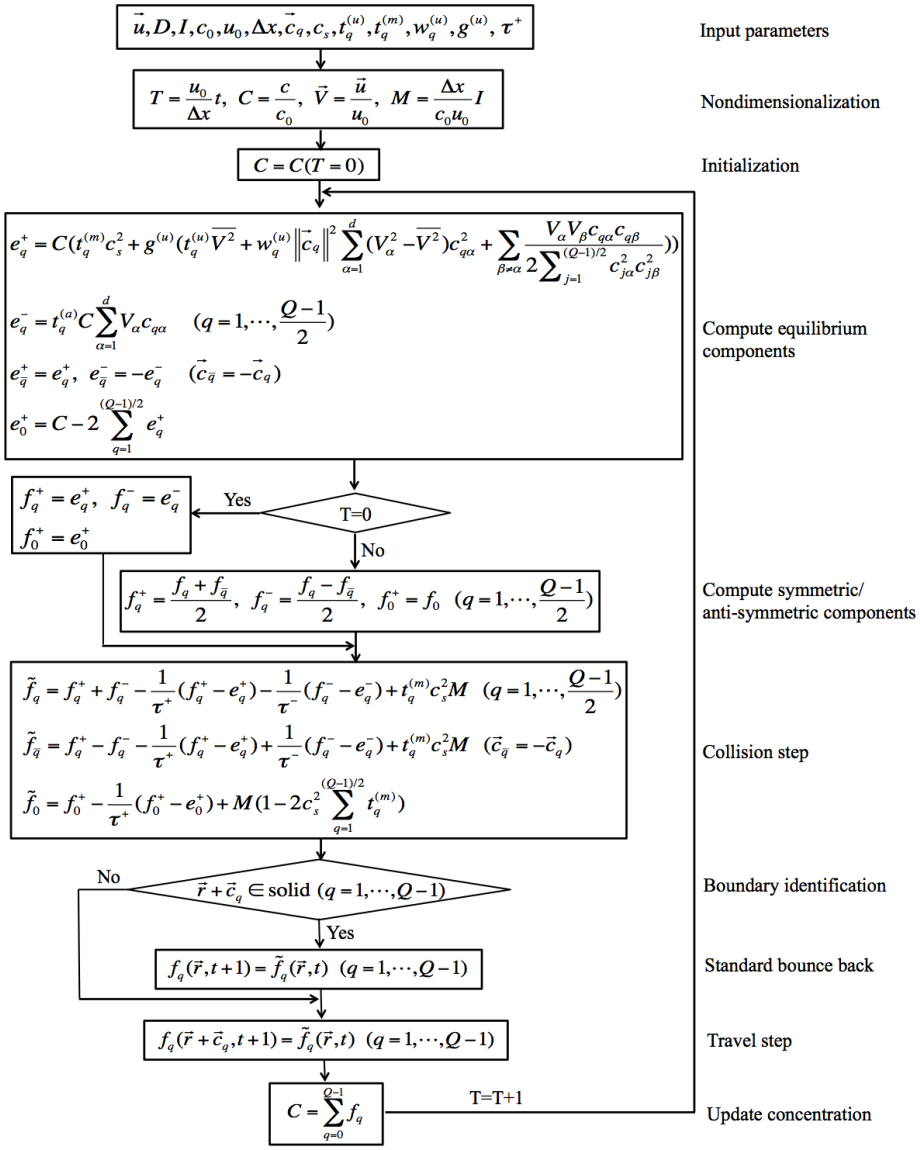

Figure 2: Pseudocode for applying the TRT LBM to reactive transport.

solute distribution. $m = 0.56$ kg/m, $x_0 = 1$ m, and $\sigma_0 = 0.22$ m were chosen in the simulations. A periodic boundary condition was applied at both ends of the domain. $\Delta x = 1 \times 10^{-3}$ m, $u_0 = 1 \times 10^{-4}$ m/s, and $c_0 = 1$ kg/m were used to normalize the dimensional ADE (eq. (12)). Different diffusion coefficients, $D = 7.5 \times 10^{-9}$, 7.5×10^{-10}, and 7.5×10^{-11} m^2/s (corresponding to $\tau^- = 0.7$, 0.52, and 0.502), were used in the simulations.

We varied the tunable parameter τ^+ to examine its effects on the numerical stability and accuracy of the TRT LBM. The maximum allowable velocity in the lattice space V_{max}, above which the simulations become unstable, was used to describe the numerical stability of the TRT method. A simulation was defined as stable when it continued converging after 5000 steps of computation. Figure 3 shows the dependence of V_{max} on τ^+ for three different diffusion coefficients (corresponding to three different τ^-). When τ^- is large ($\tau^- = 0.7$), the stability of the TRT method first increases monotonically with τ^+ to then reach optimal stability shortly before the choice of τ^+ that used in the SRT method. When τ^- is small ($\tau^- = 0.502$, 0.52), the stability of the TRT method first increases, then decreases, and then increases again as τ^+ increases; therefore there is a range of τ^+ values for which the stability deteriorates. This range is delimited by the τ^+ values of the SRT and OTRT methods. For all three τ^- the SRT and OTRT methods produced the same maximum values of V_{max} ($\sim$0.79). Once V exceeded 0.792, the TRT method became unstable. This is consistent with a theoretical analysis of the stability of the TRT method [45], according to which $V^2 \leq 1 - c_s^2$ (i.e. $V \leq 0.791$) is a necessary condition for the D1Q3 TRT LBM to be stable. Therefore, the SRT and OTRT methods have the same stabilities for 1D advective diffusion

in the simple geometry considered here.

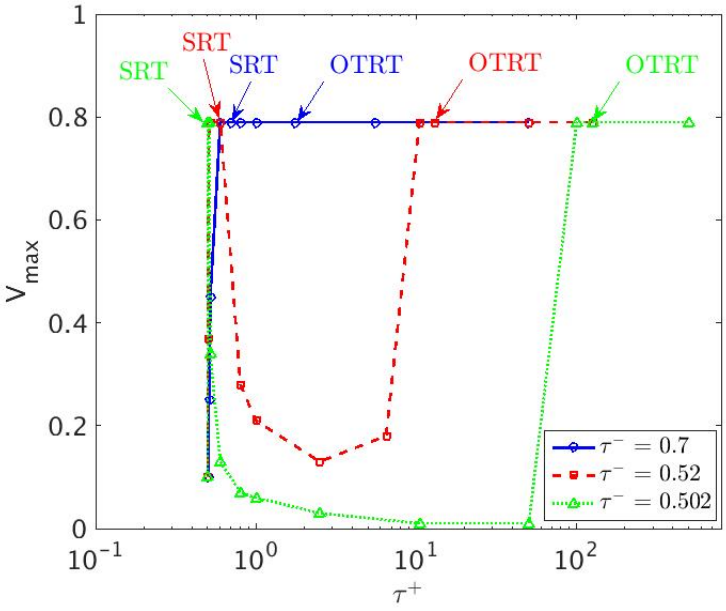

Figure 3: Dependence of stability on the tunable parameter τ^+ in simulations of 1D advection-diffusion. Three different diffusion coefficients (corresponding to different τ^-) were examined. V_{max} represents the maximum allowable velocity yielding a stable simulation (which continued converging after 5000 steps of computation). A series of τ^+ values were examined (each symbol represents the simulated V_{max} for a τ^+ value), and the two particular selections, $\tau^+ = \tau^-$ (SRT) and $\tau^+ = 1/2 + 1/(4\tau^- - 2)$ (OTRT), are indicated on the curve.

The numerical accuracy of the TRT method with different τ^+ was evaluated by comparing the simulation results with the analytical solutions (eq. 14). Table 1 shows errors of the simulated concentration produced by the TRT method for different advective velocities in lattice space V. The results show that the error generally increases with τ^+, which is expected since larger τ^+ results in larger high-order errors in the TRT simulations [46]. As

V increases, the error produced by the SRT method increases consistently for three τ^-, while that produced by the OTRT method first increases and then decreases for two smaller τ^- ($\tau^- = 0.52$, 0.502). The OTRT exhibits similar accuracy with the SRT method when $V = 0.79$. Furthermore, the error difference between the OTRT and SRT methods decreases as τ^- increases, exhibiting almost the same accuracies for all V when $\tau^- = 0.7$. Therefore, the SRT method generally produces more precise simulations than the OTRT method. However, the error difference can be ignored for large V or τ^-.

Table 1: Dependence of accuracy on the tunable parameter τ^- for different advective velocities V in simulations of 1D advection-diffusion at $t = 23$ days. Three different diffusion coefficients (corresponding to different τ^-) were examined. The accuracy is represented by relative errors (%) of the simulated solute concentration, Error $= \frac{\sum_{i=1}^{N} |C_i(\text{simulated}) - C_i(\text{analytical})|}{N C_{max}(\text{analytical})} \times 100$, where N is the number of numerical nodes along the direction of flow, $N = 2000$, C_i is the solute concentration at the location $i\Delta x$, and C_{max}(analytical) is the maximum concentration of the analytical solutions at that time. NaN denotes a numerically unstable solution.

	$\tau^- = 0.7$		$\tau^- = 0.52$					$\tau^- = 0.502$	
V	τ^+		τ^+					τ^+	
	1.75 (OTRT)	0.7 (SRT)	125.5	13 (OTRT)	2.5	0.52 (SRT)	0.502	125.5 (OTRT)	0.502 (SRT)
0.1	0.041	0.040	0.190	0.019	0.014	0.014	0.014	0.020	0.015
0.3	0.050	0.044	0.477	0.044	NaN	0.025	0.025	0.048	0.026
0.5	0.051	0.050	0.526	0.059	NaN	0.036	NaN	0.067	0.039
0.79	0.057	0.057	0.050	0.049	NaN	0.049	NaN	0.060	0.059
0.8	NaN	NaN	NaN	NaN	NaN	NaN	NaN	NaN	NaN

3.2. Taylor dispersion

Taylor dispersion in a pipe was used to further evaluate the stability and accuracy of the TRT method when solid boundaries exist. The velocity

distribution in the pipe is described by [50]:

$$u(r) = 2\overline{u}(1 - r^2/R^2) \tag{15}$$

where $\overline{u}$ is the average flow velocity, R is the radius of the pipe, and r is the radial coordinate, $r = \sqrt{y^2 + z^2}$. A slug of solute was initially injected into the pipe with diameter of 0.01 m and length of 2 m. The effective diffusion coefficient of the solute can be estimated by [51]:

$$D_e^{analytical} = D\left(1 + \frac{\mathrm{Pe}^2}{192}\right) \tag{16}$$

where Pe is Peclet number, $\mathrm{Pe} = 2\overline{u}R/D$.

The simulations used the same numerical settings and parameter values as in the previous 1D transport simulations. The stability of the TRT method was described by V_{max}. Its accuracy was evaluated by comparing $D_e^{analytical}$ with simulated values, which were calculated based on the simulated solute concentration

$$D_e^{simulated} = \frac{1}{2}\frac{d\langle\sigma^2\rangle}{dt} = \frac{1}{2}\frac{\langle\sigma_{t_2}^2\rangle - \langle\sigma_{t_1}^2\rangle}{t_2 - t_1} \tag{17}$$

where $\langle\sigma^2\rangle$ is the variance of concentration distribution. It can be estimated by

$$\langle\sigma^2(t)\rangle = \frac{\iiint (x - \langle x(t)\rangle)^2 c(x,y,z,t)dxdydz}{\iiint c(x,y,z,t)dxdydz} \tag{18}$$

where $\langle x\rangle$ is the center of solute mass along the direction of flow. It can be estimated by

$$\langle x(t)\rangle = \frac{\iiint xc(x,y,z,t)dxdydz}{\iiint c(x,y,z,t)dxdydz} \tag{19}$$

Fig. 4 shows the stability of the TRT method changed with τ^+ for different τ^-. Compared with the previous 1D transport, the stability of the SRT method considerably deteriorates due to the effects of boundaries, while the

stability of the OTRT method degrades for small τ^+ but improves for large τ^+. The OTRT method demonstrated better stability than the SRT method for all three τ^- values, with increasing stability as τ^- decreases. Fig. 4 shows that the OTRT method obtains larger V_{max} values than the SRT method especially when $\tau^- = 0.502$ ($V_{max} = 0.96$ for OTRT and 0.12 for SRT). This instability of the SRT method as τ^- approaches 0.5 is a well-known shortcoming of this method [29, 33]. Therefore, the OTRT method can improve numerical stability compared with the SRT method when simulating reactive transport in geometries with boundaries which are present in porous media. The degree of improvement increases as τ^- decreases.

Table 2 shows the accuracy of the TRT method changed with τ^+ for different τ^- (diffusion coefficient) and $\overline{V}$ ($\overline{V} = \overline{u}/u_0$). Compared with the previous 1D transport without solid boundaries, the accuracy similarly decreases with τ^+, but the value of error apparently increases for the same τ^+, τ^- and $\overline{V}$. These results illustrate that the boundaries together with the SBB boundary condition introduce significant errors to the TRT simulations. The error of the OTRT method generally increases with $\overline{V}$, but remains almost constant once it reaches about 10.5% for all the three τ^- values. In contrast, the error of the SRT method varies with $\overline{V}$ and τ^- in a more complex manner, illustrating the complicated effects of boundaries on the accuracy. Overall, the error produced by the SRT method is much smaller than that produced by the OTRT method: this is probably due to the larger dissipation in the OTRT method [46].

We further investigated the effects of boundaries on the stability and accuracy of the TRT method by changing mesh resolution N, where $N =$

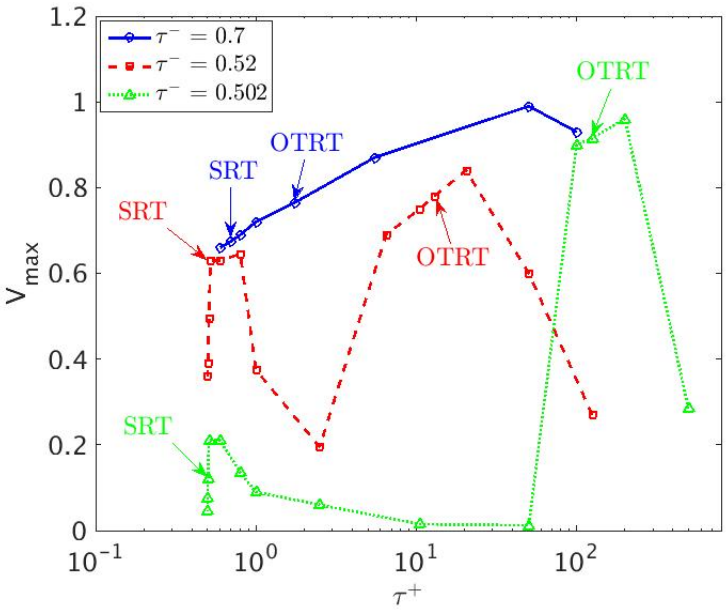

Figure 4: Dependence of stability on the tunable parameter τ^+ in simulations of Taylor dispersion. Three different diffusion coefficients (corresponding to different τ^-) were examined. V_{max} represents the maximum allowable velocity yielding a stable simulation (which continued converging after 5000 steps of computation). A series of τ^+ values were examined (each symbol represents the simulated V_{max} for a τ^+ value), and the two particular selections, $\tau^+ = \tau^-$ (SRT) and $\tau^+ = 1/2 + 1/(4\tau^- - 2)$ (OTRT), are indicated on the curve.

$2R/\Delta x$. Note that $N = 10$ in Fig. 4 and Table 2, and τ^- is a function of N, $\tau^- = 1/2 + ND/(2Rc_s^2 u_0)$. Only the SRT and OTRT methods were examined in the Taylor dispersion simulations with $Pe = 100$. Fig. 5 shows the change of V_{max} and error ϵ, $\epsilon = D_e^{simulated} - D_e^{analytical}$, with respect to N for two different D.

Table 2: Dependence of accuracy on the tunable parameter τ^- for different advective velocities V in simulations of Taylor dispersion. Three different diffusion coefficients (corresponding to different τ^-) were examined. The accuracy is represented by relative error (%) of the effective diffusion coefficient (i.e. Error $= \frac{D_e^{simulated} - D_e^{analytical}}{D_e^{simulated}} \times 100$). NaN denotes a numerically unstable solution

	$\tau^- = 0.7$			$\tau^- = 0.52$					$\tau^- = 0.502$		
$\overline{V}$	Pe	τ^+		Pe	τ^+				Pe	τ^+	
		1.75 (OTRT)	0.7 (SRT)		125.5	13 (OTRT)	2.5	0.52 (SRT)	0.502		125.5 (OTRT)	0.502 (SRT)
0.0075	1	-6.15	-2.94	10	15.73	-0.58	-0.69	-0.31	-0.30	100	10.05	5.03
0.075	10	-0.18	-0.35	100	77.14	10.05	3.51	1.41	1.39	1000	10.06	NaN
0.225	30	8.36	2.78	300	NaN	10.42	NaN	0.71	NaN	3000	10.50	NaN
0.3	40	9.63	2.78	400	NaN	10.42	NaN	0.03	NaN	4000	10.40	NaN
0.375	50	9.70	NaN	500	NaN	10.51	NaN	NaN	NaN	5000	10.66	NaN
0.45	60	NaN	NaN	600	NaN	NaN	NaN	NaN	NaN	6000	NaN	NaN

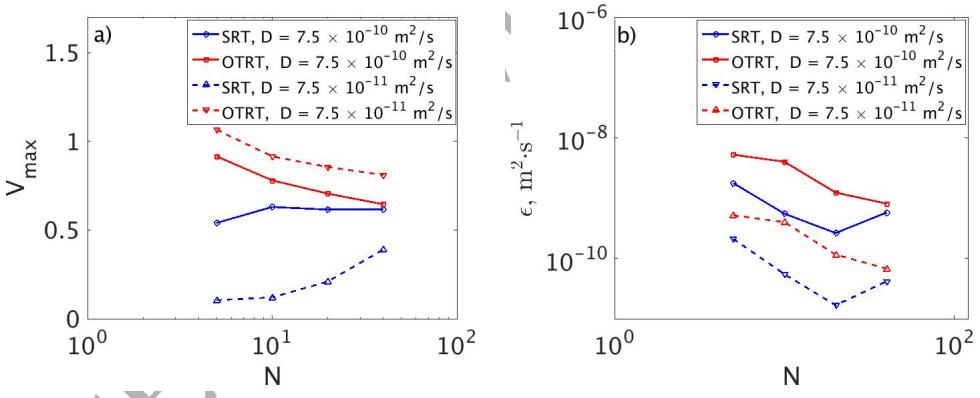

Figure 5: a) Stability of the SRT and OTRT methods with respect to mesh resolution N in simulations of Taylor dispersion. Two different diffusion coefficients D were examined.V_{max} represents the maximum allowable velocity yielding a stable simulation (which continued converging after 5000 steps of computation). b) Error of the SRT and OTRT methods with respect to mesh resolution, $\epsilon = D_e^{simulated} - D_e^{analytical}$. $Pe = 100$ in the simulations

The results show that the stability of the OTRT method degrades as N increases, although the rate of degradation decreases. By contrast, the stability of the SRT method depends on the value of D. When $D = 7.5\times10^{-11}$ m^2/s, the stability of the SRT method increases monotonically with N, although it is still inferior to that of the OTRT method for $N = 40$. When $D = 7.5\times10^{-10}$ m^2/s, the stability of the SRT method first increases with N and quickly reaches a plateau as $N \geq 10$, similar to the stability of the OTRT method when $N = 40$. This fixed stability of the SRT method probably results from its insufficient dissipation [33]. Therefore, the stability of the SRT method can be improved by refining mesh resolution, but it may fail for high resolution. The OTRT method provides better stability than the SRT method for small D, even for mesh with high resolution.

The results for accuracy in Fig. 5b show that the SRT method generally results in more precise simulations than the OTRT method. Both methods converge when $N \leq 20$, presenting a convergence speed of about 2. The SRT method stops converging as $N > 20$ while the OTRT continue to converge at these values, though its convergence speed slows down. The different convergences result in similar accuracies between the two methods when $N = 40$. The higher errors produced by the SRT method primarily results from the SBB boundary condition, which leads to uncorrected boundary location and increasing numerical errors as N becomes large [33]. In summary, the simulations of Taylor dispersion illustrate that the stability of the SRT method for τ^- approaching 0.5 can be improved by refining the spatial resolution. However, this also reduces the accuracy of this method. In contrast, the OTRT method is able to produce more accurate simulations while maintaining good

stability when the mesh resolution is refined.

3.3. Advection diffusion in a packed column

Advection-diffusion in a column packed with random monodispersed beads was used to evaluate the accuracy and stability of the TRT method in complicated geometries [52]. The length and diameter of the column are 16.8 mm and 8.8 mm, and the diameter of the beads is $L = 0.5$ mm. The flow field given in [52] was used in the transport simulations, with Darcy velocity $q_v = 4.556 \times 10^{-4}$ m/s. The solute with $c = 1$ kg/m^3 was injected into the column at the inlet along with the incoming fluid. The injection of the solute continued for 2.78 s, and all solute eventually exited the column driven by advection and dispersion. A pulse-type incoming concentration was imposed at the inlet and free exit was employed at the outlet [52]. $u_0 = 0.1$ m/s, $c_0 = 1$ kg/m^3, and $\Delta x = 4 \times 10^{-5}$ m were selected in the simulations. This spatial resolution leads to 221x221x421 total numerical voxels, and requires extensive computational resources. Therefore, we examined the stability and accuracy of the TRT method using only two particular TRT models (SRT and OTRT).

We found that the OTRT method is more stable than the SRT method, although both of them are more prone to numerical instability in the complicated geometry than in the previous simple geometries. The SRT method became unstable once $D < 4.2 \times 10^{-8}$ m^2/s ($\tau^- < 0.528$), while the OTRT method became unstable when $D < 3 \times 10^{-9}$ m^2/s ($\tau^- < 0.502$). Figure 6 shows the concentration distribution obtained by the OTRT method in a slice 10.78 s after the solute injection. $D = 2.08 \times 10^{-8}$ m^2/s ($\tau^- = 0.5139$) was used in this case. The solute plume was apparently dispersed by the

nonuniform flow pattern, with the solute near the column walls exiting the column first along the preferential flow paths. The breakthrough curve, for which the effluent solute concentration was calculated by flux-weight average values [53], was compared with the one attained by the finite volume method (FVM) reported in [52]. Figure 7 shows a good match between the simulations obtained by the OTRT and FVM. The results illustrate that the OTRT can reliably predict the dispersive transport in complicated geometries. The simulation using the SRT method for this D was unstable, and is thereby not shown. However, the accuracies of the two methods were similar to each other in simulations with larger D ($D > 4.2\times10^{-8}$ m^2/s), where both the SRT and OTRT methods were stable.

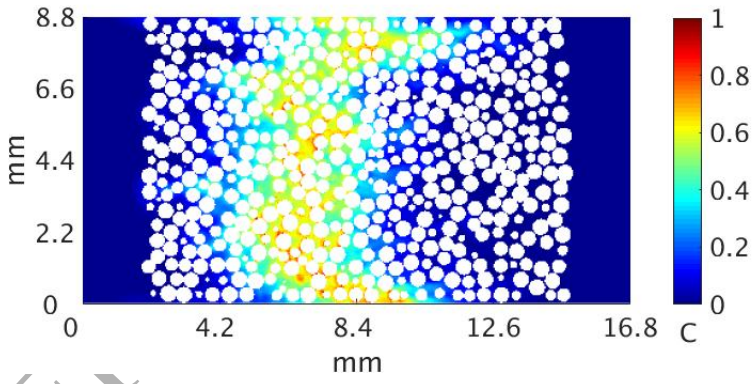

Figure 6: Concentration distribution in a slice of the 3D packed column, 10.78 s after the solute injection. $D = 2.08\times10^{-8}$ m^2/s ($\tau^- = 0.5139$) was used in the simulation. The concentration was normalized by the concentration of the injected solute

For the packed column, the Knudsen number (K_n), the ratio of the mean free path of molecules to a characteristic flow length, was calculated to evaluate the effects of small pore size on flow and transport in the column [20].

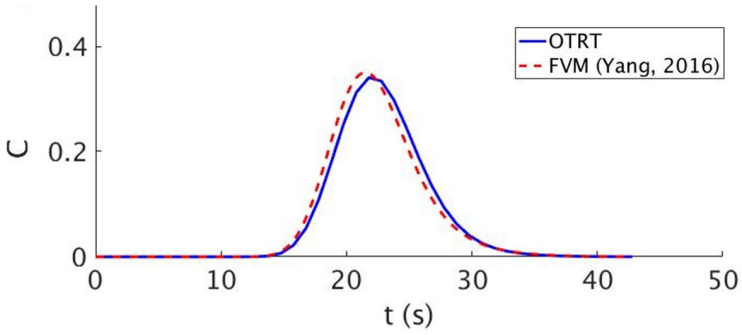

Figure 7: Comparisons of breakthrough curves at the outlet of the column obtained by the OTRT method against the one obtained by finite volume method (FVM) reported in [52].

We found the K_n value is much smaller than 1, $K_n = \sqrt{\frac{\pi}{2}}\frac{\nu}{L}$=0.0025 [54], so the continuum flow and transport equations such as equation (12) can be used to describe the physical and chemical processes in the column [55]. Given the small values of K_n in this and other cases, we neglected the effects of Knudsen layer on the stability and accuracy of the TRT method [56].

3.4. Reactive transport in uniform flow

One-dimensional reactive transport in uniform flow was used to evaluate the stability and accuracy of the TRT method in simulating reactive transport. With a first-order reaction term ($I = -kc$), zero initial concentration ($c(x \geq 0, 0) = 0$), and fixed concentration at the inlet of a semi-infinite domain ($c(x = 0, t) = c_0$), eq. (12) yields the following analytical solutions [57]:

$$c(x,t) = \frac{c_0}{2}\exp\frac{vx}{2D}\left[\exp(-\beta x)\mathrm{erfc}(\frac{x-(v^2+4kD)^{1/2}t}{2(Dt)^{1/2}}) + \exp(\beta x)\mathrm{erfc}(\frac{x+(v^2+4kD)^{1/2}t}{2(Dt)^{1/2}})\right] \tag{20}$$

where k is the reaction rate constant, $\beta = (v^2/4D^2 + k/D)^{1/2}$, and $\mathrm{erfc}(x) = 1 - \mathrm{erf}(x) = \frac{2}{\sqrt{\pi}} \int_x^\infty \exp(-\tau^2) d\tau$. Consequently, $M = -kC\Delta x/u_0$ in eq. (11); M was computed explicitly using the known C values at the previous step during the simulations. The simulations employed the same numerical settings as in the previous 1D non-reactive transport.

Figure 8 shows the comparison between the simulated concentration obtained by the TRT method with different τ^+ and the analytical solutions for different k when $\tau^- = 0.52$. The results show that the TRT method reliably predicts the reactive transport for a wide range of reaction rates, although the error slightly increases with τ^+. The effects of τ^- on the accuracy and stability are similar to those in the previous 1D advection-diffusion and are thereby not present. Therefore, the TRT method provides reliable predictions for the reactive transport in simple geometries.

3.5. Bacterial chemotaxis in two-dimensional porous media

Contaminant degradation by chemotactic bacteria in two-dimensional porous media was used to illustrate the applications of the TRT method to biogeochemical reactions in subsurface environments. Chemotaxis enables motile bacteria to move toward contaminants with high concentration, thereby accelerating the removal of contaminants [58, 59]. We assume that the transport and fate of bacteria can be described by an reactive ADE and that the contaminant is the only rate-limiting substrate. Thus the transport and fate of the bacteria and contaminant can be described by [60]:

$$\begin{aligned} \frac{\partial c_b}{\partial t} + \nabla \cdot [c_b(\mathbf{u} + \mathbf{u}_c) - D_b \nabla c_b] &= Y q_b \frac{c_c}{c_c + K_c} c_b - k_b c_b \\ \frac{\partial c_c}{\partial t} + \nabla \cdot (c_c \mathbf{u} - D_c \nabla c_c) &= -q_b \frac{c_c}{c_c + K_c} c_b \end{aligned} \tag{21}$$

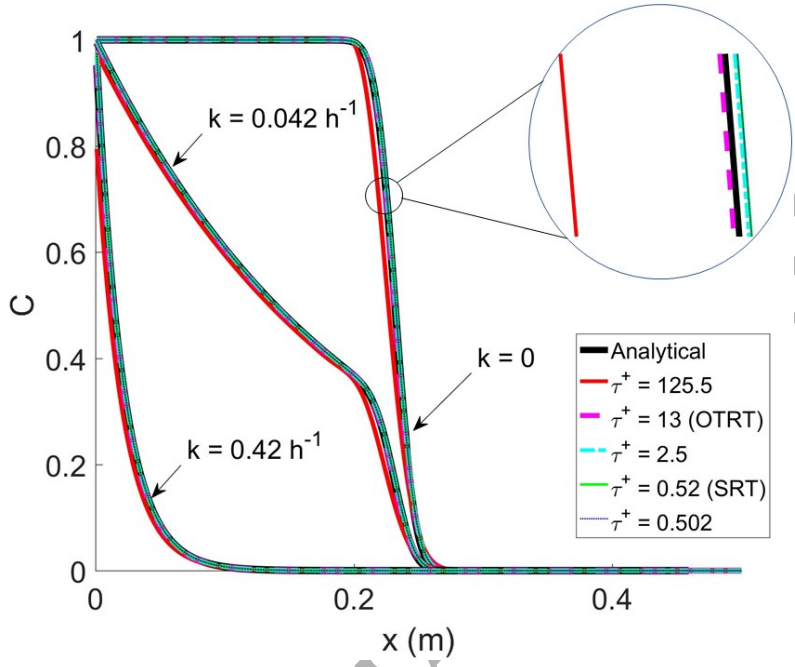

Figure 8: Comparison between the simulated concentration obtained by the TRT method with different τ^+ and the analytical solutions for 1D reactive transport at $t = 27.8$ hours. Different reaction rate constants k were examined, and $D = 7.5\times10^{-10}$ m^2/s ($\tau^- = 0.52$).

where c_b is the bacterial concentration, c_c is the contaminant concentration, D_b is the random motility coefficient of the bacteria, D_c is the diffusion coefficient of the contaminant, q_b is the maximum reaction rate of the contaminant, K_c is the half-saturation coefficient, Y is the yield coefficient, k_b is the decay rate, and $\mathbf{u}_c$ is chemotactic velocity. $\mathbf{u}_c$ depends on the contaminant concentration as well as its gradient, and can be described by [61]:

$$\mathbf{u}_c = \frac{2v_{swim}}{3}\tanh\left(\frac{\chi_0}{2v_{swim}}\frac{K_d}{(K_d+c_c)^2}|\nabla c_c|\right)\frac{\nabla c_c}{|\nabla c_c|} \tag{22}$$

where v_{swim} is the swimming speed of the bacteria, K_d is a dissociation constant, and χ_0 is the chemotactic sensitivity coefficient. The values of parameters v_{swim}, K_d, and χ_0 depend on a number of factors including bacteria species, buffer solution chemistry, and temperature [62], and affect the transport rate of bacteria in porous media through altering the value of the chemotactic velocity $\mathbf{u}_c$. This chemotactic velocity modifies the advective velocity in lattice space, $\mathbf{V} = (\mathbf{u} + \mathbf{u}_c)/u_0$, in the application of TRT simulations, such that the effects of chemotaxis could be considered in the reactive ADE (eq. 12).

The bacteria were initially injected into a cavity in the porous media, while the contaminant was uniformly distributed in the beginning. The bacteria degraded the contaminant during its movement, driven by advection, diffusion, and chemotaxis [34]. The parameter values used in the chemotactic system are presented in Table 3, in which the values were estimated based on an experiment of bacterial chemotaxis in a capillary tube [58]. A hospitable environment and necessary nutrients, such as sodium (Na), potassium (K), and phosphate buffer (pH = 7), were provided in the experiment, so that the bacteria could grow and exhibit chemotaxis [58, 62, 63]. The fluid field simulated by the MRT method in [34] was used in the transport simulations, in which Darcy velocity $q_v = 3.2 \times 10^{-6}$ m/s. $\Delta x = 1.5 \times 10^{-5}$ m and $u_0 = 4.8 \times 10^{-5}$ m/s were chosen in the simulations.

Only the SRT and OTRT methods were used in the application, and their stability and accuracy were examined by varying the bacterial random motility coefficient D_b, which changes τ^- (i.e. $\tau^- = 1/2 + D_b/(c_s^2 \Delta x u_0)$). The simulations showed that the OTRT has a better numerical stability than the

Table 3: Parameter values used in the chemotactic system [58, 34]

Symbol	Description	Value
c_b	Initial bacterial concentration	4×10^8 cfu/ml
c_c	Initial contaminant concentration	2.8×10^{-2} g/ml
D_c	Diffusion coefficient of contaminant	7.5×10^{-6} cm^2/s
q_b	Maximum reaction rate of contaminant	7.9×10^{-13} g/cfu/s
Y	Yield coefficient	0
k_d	Decay rate	0
K_c	Half-saturation coefficient of contaminant	1.3×10^{-4} g/ml
K_d	Dissociation constant	2.1×10^{-3} g/ml
χ_0	Chemotactic sensitivity coefficient	1.8×10^{-5} cm^2/s
v_{swim}	Bacterial swimming speed	4.8×10^{-3} cm/s

SRT method; i.e. the SRT method became unstable at $D_b < 8 \times 10^{-12}$ m^2/s ($\tau^- < 0.530$) while the OTRT method became unstable at $D_b < 3.2 \times 10^{-12}$ m^2/s ($\tau^- < 0.512$). Compared with the previous simulations of reactive transport in simple geometries, the SRT and OTRT methods are easier to become unstable in the complicated geometry.

The accuracies of the SRT and TRT methods were evaluated by comparing their simulation results with those obtained by the MRT method reported in [34]. Fig. 9 shows the simulated bacterial distributions obtained by the three methods for $D_b = 3.2 \times 10^{-11}$ m^2/s. We find that both the SRT and OTRT methods reliably predicted bacterial distributions, although they overestimated the concentration in the cavity (see Fig. 9e). A portion of

the bacteria separated from the original injection slug and formed a moving ring with a high concentration. This ring was caused by chemotaxis and enables the bacteria to access and degrade more contaminants than the bacteria without chemotaxis. Overall, both the SRT and OTRT methods are able to produce results that are comparative to those obtained by the MRT method. Compared with the MRT method, in which the mathematical presentation is complex and the selection of relaxation parameters is challenging, the TRT method described here is easier to implement.

4. Conclusions

This study clearly describes the framework and implementation of the TRT LBM. This method was then applied to various advective-diffusive-reactive transport in simple and complicated geometries, and demonstrated its ability to reliably predict a broad range of transport phenomena. The fact that one of the two relaxation parameters in the TRT LBM is tunable enables the TRT method to produce robust numerical performances in terms of accuracy and stability. The selection of the tunable parameter, τ^+, is important for the accuracy and stability of the TRT LBM. Generally, the accuracy of the TRT method increases as τ^+ decreases while the stability depends on the values of τ^+ and the other relaxation parameter τ^-. When τ^- approaches 0.5, the TRT method is prone to numerical instability when a small τ^+ is selected, which is the case for the SRT method. The TRT method can attain much better stability when large τ^+ is selected, which is the case for the OTRT method. Therefore, although the numerical accuracy might be exacerbated, the TRT LBM can be applied to simulate a broader range

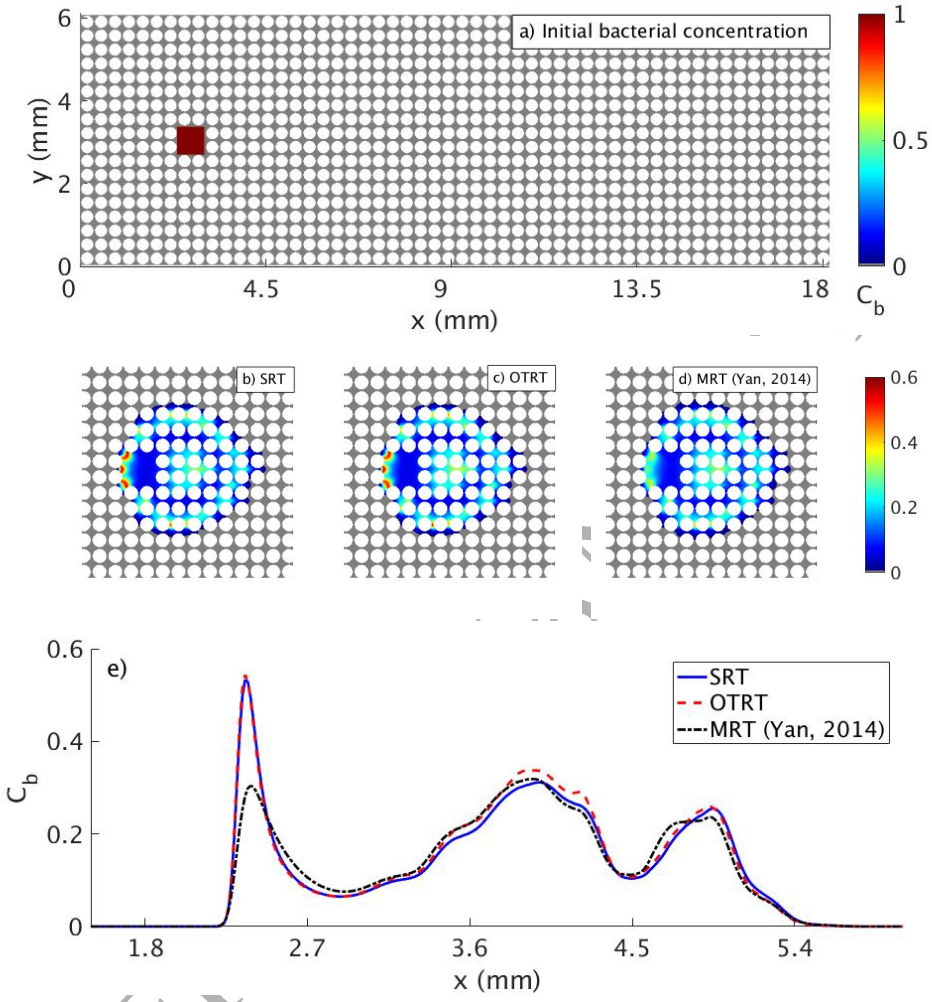

Figure 9: a) Initial distribution of bacterial concentration. b-d) Distributions of the simulated bacterial concentration obtained by SRT, OTRT, and MRT [34] around the injection cavity at t = 0.26 hours. e) Distributions of the simulated bacterial concentration along the centerline parallel to the direction of flow (y = 3 mm). The bacterial concentration, C_b, was normalized by the injecting bacterial concentration.

of transport phenomena than the SRT LBM, such as transport with large advective velocity and/or small diffusion coefficient in complicated geometries, through tuning τ^+ and thereby improving the numerical stability. To summarize, the TRT LBM can reliably predict various advective-diffusive-reactive transport in both simple and complicated geometries by choosing an appropriate value of τ^+. This study demonstrates the significant potential of the TRT LBM in predicting various geophysical and biogeochemical processes in subsurface environments.

5. Acknowledgments

This work was supported by US National Science Foundation (NSF) through Grant No 0911425, US National Institute of Health (NIH) through Grant No. P30 ES009089, and the Ministry of Science and Technology of China through Grant No. 2016YFA0601000. This research was also supported by the US Department of Energy (DOE) Biological and Environmental Research (BER) Division, Subsurface Biogeochemical Research (SBR) program, through the PNNL SBR Scientific Focus Area project. PNNL is operated by Battelle Memorial Institute under subcontract DE-AC06-76RLO 1830. We would like to express our sincere gratitude to Dr. Irina Ginzburg for providing countless insightful suggestions and for her help with performing the simulations. We also would like to thank Dr. Sandra Taylor for her helpful edit. The source code for the method used in this study is written by the authors. This code together with input files necessary to reproduce the simulation results are available from the authors upon request (yanzf14@outlook.com).

References

[1] I. Nambi, W. C.J., S. R.A., V. A.J., Pore-scale analysis of anaerobic halorespiring bacterial growth along the transverse mixing zone of an etched silicon pore network, Environmental Science and Technology 37 (2003) 5617–5624.

[2] P. Meakin, A. Tartakovsky, Modeling and simulation of porescale multiphase fluid flow and reactive transport in fractured and porous media, Reviews of Geophysics 47.

[3] X. Wang, T. Long, Bacterial chemotaxis toward a NAPL source within a pore-scale microfluidic chamber, Biotechnology and Bioengineering 109 (7) (2012) 1622–1628.

[4] Z. Yan, C. Liu, K. E. Todd-Brown, Y. Liu, B. Bond-Lamberty, V. L. Bailey, Pore-scale investigation on the response of heterotrophic respiration to moisture conditions in heterogeneous soils, Biogeochemistry.

[5] M. Blunt, B. Bijeljic, H. Dong, O. Gharbi, S. Iglauer, P. Mostaghimi, A. Paluszny, C. Pentland, Pore-scale imaging and modelling, Advances in Water Resources 51 (2013) 197–216.

[6] H. Yoon, Q. Kang, A. J. Valocchi, Lattice boltzmann-based approaches for pore-scale reactive transport, Reviews in Mineralogy and Geochemistry 80 (1) (2015) 393–431.

[7] S. Chen, G. Doolen, Lattice Boltzmann method for fluid flows, Annual Review of Fluid Mechanics 30 (1998) 329–364.

[8] W. Long, M. Hilpert, Lattice-Boltzmann modeling of contaminant degradation by chemotactic bacteria: Exploring the formation and movement of bacterial bands, Water Resources Research 44 (2008) W09415.

[9] C. Aidun, J. Clausen, Lattice-Boltzmann method for complex flows, Annual Review of Fluid Mechanics 42 (2010) 439–472.

[10] H. Liu, Q. Kang, C. R. Leonardi, S. Schmieschek, A. Narvaez, B. D. Jones, J. R. Williams, A. J. Valocchi, J. Harting, Multiphase Lattice Boltzmann Simulations for Porous Media Applications, Computational Geosciences 20 (4) (2016) 777–805.

[11] A. Calì, S. Succi, A. Cancelliere, R. Benzi, M. Gramignani, Diffusion and hydrodynamic dispersion with the lattice boltzmann method, Physical Review A 45 (1992) 5771–5774.

[12] R. Parales, J. Ditty, C. Harwood, Toluene-degrading bacteria are chemotactic towards the environmental pollutants benzene, toluene, and trichloroethylene., Applied and Environmental Microbiology 66 (9) (2000) 4098–4104.

[13] Z. Yan, E. Bouwer, M. Hilpert, Coupled effects of chemotaxis and growth on traveling bacterial waves, Journal of Contaminant Hydrology 164 (2014) 138–152.

[14] Q. Kang, P. Lichtner, H. Viswanathan, Pore Scale Modeling of Reactive Transport Involved in Geologic CO2 Sequestration, Transport in Porous Media.

[15] Z. Tian, H. Xing, Y. Tan, J. Gao, A coupled lattice boltzmann model for simulating reactive transport in co2 injection, Physica A: Statistical Mechanics and its Applications 403 (2014) 155 – 164.

[16] Q. Kang, D. Zhang, S. Chen, X. He, Lattice boltzmann simulation of chemical dissolution in porous media, Physical Review E 65 (3) (2002) 036318.

[17] Q. Kang, D. Zhang, S. Chen, Simulation of dissolution and precipitation in porous media, Journal of Geophysical Research: Solid Earth 108 (B10).

[18] L. Chen, Q. Kang, H. S. Viswanathan, W.-Q. Tao, Pore-scale study of dissolution-induced changes in hydrologic properties of rocks with binary minerals, Water Resources Research 50 (12) (2014) WR015646.

[19] Q. Li, K. Luo, Q. Kang, Y. He, Q. Chen, Q. Liu, Lattice boltzmann methods for multiphase flow and phase-change heat transfer, Progress in Energy and Combustion Science 52 (2016) 62 – 105.

[20] A. Montessori, P. Prestininzi, M. La Rocca, S. Succi, Lattice boltzmann approach for complex nonequilibrium flows, Phys. Rev. E 92 (2015) 043308.

[21] G. Falcucci, S. Succi, A. Montessori, S. Melchionna, P. Prestininzi, C. Barroo, D. C. Bell, M. M. Biener, J. Biener, B. Zugic, Mapping reactive flow patterns in monolithic nanoporous catalysts, Microfluidics and Nanofluidics 20 (7) (2016) 1–13.

[22] A. Montessori, P. Prestininzi, M. L. Rocca, G. Falcucci, S. Succi, E. Kaxiras, Effects of knudsen diffusivity on the effective reactivity of nanoporous catalyst media, Journal of Computational Science 17, Part 2 (2016) 377 – 383, discrete Simulation of Fluid Dynamics 2015.

[23] G. Falcucci, G. Amati, V. K. Krastev, A. Montessori, G. S. Yablonsky, S. Succi, Heterogeneous catalysis in pulsed-flow reactors with nanoporous gold hollow spheres, Chemical Engineering Science 166 (2017) 274 – 282.

[24] R. Benzi, S. Succi, M. Vergassola, The lattice boltzmann equation: theory and applications, Physics Reports 222 (3) (1992) 145 – 197.

[25] F. Higuera, S. Succi, R. Benzi, Lattice gas dynamics with enhanced collisions, EPL (Europhysics Letters) 9 (4) (1989) 345.

[26] Z. Guo, C. Shu, Lattice Boltzmann method and its applications in engineering (advances in computational fluid dynamics), World Scientific Publishing Company, 2013.

[27] S. Succi, The lattice Boltzmann equation: for fluid dynamics and beyond, Oxford university press, 2001.

[28] D. Groen, J. Hetherington, H. B. Carver, R. W. Nash, M. O. Bernabeu, P. V. Coveney, Analysing and modelling the performance of the hemelb lattice-boltzmann simulation environment, Journal of Computational Science 4 (5) (2013) 412–422.

[29] X. He, Q. Zou, L. Luo, M. Dembo, Analytic solutions of simple flows

and analysis of nonslip boundary conditions for the lattice Boltzmann BGK model, Journal of Statistical Physics 87 (1-2) (1997) 115–136.

[30] C. Pan, L. Luo, C. Miller, An evaluation of lattice Boltzmann schemes for porous medium flow simulation, Computers and Fluids 35 (8-9) (2006) 898–909.

[31] Q. Kang, P. C. Lichtner, D. Zhang, Lattice boltzmann pore-scale model for multicomponent reactive transport in porous media, Journal of Geophysical Research: Solid Earth 111 (B5), b05203.

[32] L. Chen, Q. Kang, Q. Tang, B. A. Robinson, Y.-L. He, W.-Q. Tao, Pore-scale simulation of multicomponent multiphase reactive transport with dissolution and precipitation, International Journal of Heat and Mass Transfer 85 (2015) 935–949.

[33] L.-S. Luo, W. Liao, X. Chen, Y. Peng, W. Zhang, Numerics of the lattice boltzmann method: Effects of collision models on the lattice boltzmann simulations, Physical Review E 83 (5) (2011) 056710.

[34] Z. Yan, M. Hilpert, A multiple-relaxation-time lattice-boltzmann model for bacterial chemotaxis: effects of initial concentration, diffusion, and hydrodynamic dispersion on traveling bacterial bands, Bulletin of Mathematical Biology 76 (10) (2014) 2449–75.

[35] D. d'Humières, I. Ginzburg, M. Krafczyk, P. Lallemand, L. Luo, Multiple-relaxation-time lattice Boltzmann models in three dimensions, Philosophical Transactions of The Royal Society of London Series A 360 (1792) (2002) 437–451.

[36] I. Ginzburg, Equilibrium-type and link-type lattice Boltzmann models for generic advection and anisotropic-dispersion equation, Advances in Water Resources 28 (11) (2005) 1171–1195.

[37] I. Ginzburg, Generic boundary conditions for lattice Boltzmann models and their application to advection and anisotropic dispersion equations, Advances in Water Resources 28 (11) (2005) 1196–1216.

[38] L. Talon, D. Bauer, N. Gland, S. Youssef, H. Auradou, I. Ginzburg, Assessment of the two relaxation time lattice-boltzmann scheme to simulate stokes flow in porous media, Water Resources Research 48 (4) (2012) W04526.

[39] A. Genty, V. Pot, Numerical simulation of 3d liquid–gas distribution in porous media by a two-phase trt lattice boltzmann method, Transport in Porous Media 96 (2) (2013) 271–294.

[40] H. Liu, A. J. Valocchi, C. Werth, Q. Kang, M. Oostrom, Pore-scale Simulation of Liquid CO2 Displacement of Water Using a Two-phase Lattice Boltzmann Model, Advances in Water Resources 73 (2014) 144–158.

[41] B. Servan-Camas, F. T.-C. Tsai, Lattice boltzmann method with two relaxation times for advection–diffusion equation: third order analysis and stability analysis, Advances in Water Resources 31 (8) (2008) 1113–1126.

[42] A. Genty, V. Pot, Numerical calculation of effective diffusion in unsatu-

rated porous media by the trt lattice boltzmann method, Transport in Porous Media 105 (2) (2014) 391–410.

[43] L. Li, K. Maher, A. Navarre-Sitchler, J. Druhan, C. Meile, C. Lawrence, J. Moore, J. Perdrial, P. Sullivan, A. Thompson, et al., Expanding the role of reactive transport models in critical zone processes, Earth-Science Reviews.

[44] I. Ginzburg, F. Verhaeghe, D. d'Humières, Two-relaxation-time lattice Boltzmann scheme: About parametrization, velocity, pressure and mixed boundary conditions, Communications in Computational Physics 3 (2) (2008) 427–478.

[45] I. Ginzburg, D. d'Humieres, A. Kuzmin, Optimal stability of advection-diffusion lattice Boltzmann models with two relaxation times for positive/negative equilibrium, Journal of Statistical Physics 139 (6) (2010) 1090–1143.

[46] I. Ginzburg, Truncation errors, exact and heuristic stability analysis of Two-Relaxation-Times lattice Boltzmann schemes for anisotropic advection-diffusion equation, Communications in Computational Physics 11 (2012) 1439–1502.

[47] I. Ginzburg, Multiple anisotropic collisions for advection-diffusion Lattice Boltzmann schemes, Advances in Water Resources 51 (2013) 381–404.

[48] Q. Zou, X. He, On pressure and velocity boundary conditions for the lattice boltzmann bgk model, Physics of Fluids 9 (6) (1997) 1591–1598.

[49] B. H. Devkota, J. Imberger, Lagrangian modeling of advection-diffusion transport in open channel flow, Water Resources Research 45 (12) (2009) W12406.

[50] S. P. Sutera, R. Skalak, The history of poiseuille's law, Annual Review of Fluid Mechanics 25 (1) (1993) 1–20.

[51] G. Taylor, Dispersion of soluble matter in solvent flowing slowly through a tube, Proceedings of the Royal Society of London Series A 219 (1953) 186–203.

[52] X. Yang, Y. Mehmani, W. A. Perkins, A. Pasquali, M. Schnherr, K. Kim, M. Perego, M. L. Parks, N. Trask, M. T. Balhoff, M. C. Richmond, M. Geier, M. Krafczyk, L.-S. Luo, A. M. Tartakovsky, T. D. Scheibe, Intercomparison of 3d pore-scale flow and solute transport simulation methods, Advances in Water Resources 95 (2016) 176 – 189.

[53] S. Molins, D. Trebotich, C. I. Steefel, C. Shen, An investigation of the effect of pore scale flow on average geochemical reaction rates using direct numerical simulation, Water Resources Research 48 (3), w03527.

[54] S. Jennings, The mean free path in air, Journal of Aerosol Science 19 (2) (1988) 159 – 166.

[55] K. H. LUO, J. XIA, E. MONACO, Multiscale modeling of multiphase flow with complex interactions, Journal of Multiscale Modelling 1 (01) (2009) 125–156.

[56] Accuracy of higher-order lattice boltzmann methods for microscale flows

with finite knudsen numbers, Journal of Computational Physics 227 (19) (2008) 8655 – 8671.

[57] J. Bear, Hydraulics of groundwater, McGraw-Hill International Book Co., 1979.

[58] R. Marx, M. Aitken, Quantification of chemotaxis to naphthalene by pseudomonas putida G7, Applied and Environmental Microbiology 65 (1999) 2847–2852.

[59] G. Alexandre, S. Greer-Phillips, I. Zhulin, Ecological role of energy taxis in microorganisms, FEMS Microbiology Reviews 28 (1) (2004) 113–126.

[60] M. Hilpert, Lattice-Boltzmann model for bacterial chemotaxis, Journal of Mathematical Biology 51 (2005) 302–332.

[61] M. Rivero, R. Tranquillo, H. Buettner, D. Lauffenburger, Transport models for chemotactic cell populations based on individual cell behaviour, Chemical Engineering Science 44 (12) (1989) 2881–2897.

[62] R. Singh, M. S. Olson, Application of Bacterial Swimming and Chemotaxis for Enhanced Bioremediation, Springer Netherlands, 2008.

[63] N. Jannelli, R. A. Nastro, V. Cigolotti, M. Minutillo, G. Falcucci, Low ph, high salinity: Too much for microbial fuel cells?, Applied Energy 192 (2017) 543 – 550.